HHS Public Access

Author manuscript

Hepatology. Author manuscript; available in PMC 2018 October 01.

Published in final edited form as:

Hepatology. 2017 October ; 66(4): 1183–1196. doi:10.1002/hep.29209.

H19 promotes cholestatic liver fibrosis by preventing ZEB1-mediated inhibition of EpCAM

Yongfeng Song[1,2,*], **Chune Liu**[1,*], **Xia Liu**[3], **Jocelyn Trottier**[4], **Michele Beaudoin**[1], **Li Zhang**[1], **Chad Pope**[5], **Guangyong Peng**[3], **Olivier Barbier**[4], **Xiaobo Zhong**[5], **Linheng Li**[6], and **Li Wang**[1,7,8,9,#]

[1]Department of Physiology and Neurobiology, and Institute for Systems Genomics, University of Connecticut, Storrs, CT 06269

[2]Department of Endocrinology and metabolism, Shandong Provincial Hospital affiliated to Shandong University, Jinan, Shandong 250021, China

[3]Division of Infectious Diseases, Allergy & Immunology, Saint Louis University School of Medicine, St. Louis, MO 63104

[4]Laboratory of Molecular Pharmacology, CHU-Québec Research Centre and Faculty of Pharmacy, Laval University, Québec, QC, Canada

[5]Department of Pharmaceutical Sciences, School of Pharmacy, University of Connecticut, Storrs, CT 06269

[6]Stowers Institute for Medical Research, Kansas City, MO 64110

[7]Department of Internal Medicine, Section of Digestive Diseases, Yale University, New Haven, CT 06520

[8]Veterans Affairs Connecticut Healthcare System, West Haven, CT 06516

[9]School of Pharmaceutical Sciences, Wenzhou Medical University, Wenzhou, Zhejiang 325035, China

Abstract

Based on our recent finding that disruption of bile acid (BA) homeostasis in mice results in the induction of hepatic lncRNA H19 expression, we sought to elucidate the role of H19 in cholestatic liver fibrosis. Hepatic overexpression of *H19* RNA augmented bile duct ligation (BDL)-induced liver fibrosis, which was accompanied by the elevation of serum ALT, AST, bilirubin, and BA levels. Multiple genes related to liver fibrosis, inflammation, and biliary hyperplasia were increased in H19-BDL vs Null-BDL mice, whereas genes in BA synthesis were decreased. Livers and spleens of H19-BDL mice showed significant enrichment of CD3+γδ+, IL-4, and IL-17 producing CD4+ and CD8+ immune cell populations. H19 downregulated hepatic zinc finger E-

[#]Correspondence: Li Wang, Ph.D., 75 North Eagleville Rd., U3156, Storrs, CT 06269. li.wang@uconn.edu; Tel: 860-486-0857; Fax: 860-486-3303.

[*]These authors contributed equally to this study.

Competing interests

All authors have nothing to declare.

box-binding homeobox 1 (ZEB1) but upregulated epithelial cell adhesion molecule (EpCAM) and SRY (sex determining region Y)-box 9 (SOX9) expression. Mechanistically, ZEB1 repressed EpCAM promoter activity and gene transcription. *H19*RNA impeded ZEB1's inhibitory action by interacting with ZEB1 protein to prevent its binding to the EpCAM promoter. Hepatic overexpression of ZEB1 or knockdown of EpCAM diminished H19-induced fibrosis; the latter was also prevented in *H19*$^{-/-}$ mice. *H19*RNA was markedly induced by bile acids in mouse small cholangiocytes (MSC) and to a lesser extent in mouse large cholangiocytes (MLC). The upregulation of *H19*RNA and EpCAM correlated positively with the downregulation of ZEB1 in primary sclerosing cholangitis (PSC) and primary biliary cirrhosis (PBC) liver specimens. Conclusions: The activation of hepatic *H19*RNA promoted cholestatic liver fibrosis in mice through the ZEB1/EpCAM signaling pathway.

Keywords

Cholangiocytes; biliary fibrosis; bile duct; ductular proliferation; long non-coding RNA

Introduction

Bile acids (BAs) can facilitate intestinal absorption and transportation of lipids and other nutrients. Impairment of bile formation or bile flow to the gallbladder and duodenum results in cholestatic liver disease (1). Cholestatic liver fibrosis develops due to the activation of matrix-producing hepatic stellate cells (HSCs), which is signified by excessive extracellular matrix deposition and HSCs differentiation into myofibroblast-like cells (2). Surgical ligation of the common bile duct (BDL) is a commonly used model to induce obstructive cholestatic injury in rodents, which disrupts bile flow and results in the accumulation of BAs in the liver (3).

Long non-coding RNAs (lncRNAs) represent a group of transcripts that are above 200 nucleotides in length but without protein coding potential. As one of the first identified lncRNAs, the H19 gene is paternally imprinted, therefore is only transcribed from the maternally inherited allele (4). H19 has been recognized with a broad spectrum of functions in multiple physiological and pathological processes (4). However, its regulatory function in the liver remains largely unknown. Our recent study showed that hepatic *H19*RNA was drastically induced in Bcl2-induced cholestatic liver injury as well as in human liver specimens from patients with fibrosis and cirrhosis (5), indicating a clinically relevant regulatory role of H19 in chronic liver disease.

Zinc finger E-box binding homeobox 1 (ZEB1) is a transcriptional repressor that has been implicated in epithelial-to-mesenchymal transition (EMT) during tissue fibrosis (6). ZEB1 inhibits E-cadherin and plays a major role in triggering EMT during organ fibrosis and cancer cell metastasis (7). Its expression is controlled by microRNA-200 family (6) and modulated by nuclear receptors small heterodimer partner (SHP) and liver receptor homolog-1 (LRH-1) (8). Interestingly, the H19 gene transcription is inhibited by SHP (5); a critical negative regulator of BA synthesis and cholestasis (9, 10) and that H19 is also

involved in the regulation of EMT (11). These studies suggest a potential cross-talk between H19 and ZEB1 in the control of cholestatic liver fibrosis.

The epithelial cell adhesion molecule (EpCAM, also known as CD326) is a homophilic Ca2+-independent cell-cell adhesion molecule that is expressed in many human epithelial tissues. It is a transmembrane glycoprotein that is frequently overexpressed in embryonic stem cells, tissue progenitors, carcinomas and cancer-initiating cells (12). EpCAM is associated with enhanced cell proliferation and it transmits signals into nucleus through intramembrane proteolysis (RIP) to release and promote nucleus translocation of its intracellular domain EpICD (13, 14). Despite intensive studies focusing on the role of EpCAM in various cancers, little is known about its regulation by lncRNA. Interestingly, in a rodent model of HCC induced by diethylnitrosamine (DEN) and carbon tetrachloride (CCl4), both *H19*RNA and EpCAM mRNA were increased in liver tumors (15). This raises the possibility for a common pathway regulated by H19 and EpCAM in liver disease.

The present study was undertaken to understand the function of H19 in cholestasis. Our study identified a H19/ZEB1/EpCAM cascade as a new regulatory module to control the development of cholestatic liver injury and fibrosis.

Materials and Methods

Animals and human liver specimens

C57BL/6 mice were purchased from the Jackson Laboratory. *H19*$^{-/-}$ mice were kindly provided by Dr. Linheng Li (16). Because H19 is a paternal imprinted gene, maternal *H19*-deleted mice were used for experiments and paternal *H19*-deleted mice were used as negative controls (neg. con.). Mice were fed a standard rodent chow diet (Harlan No. 2018) with free access to water and maintained in a 12 h light/dark (LD) cycle (light on 6 AM to 6 PM), temperature-controlled (23°C), and pathogen-free facility. *In vivo* experiments were performed on male mice at the age of 6 weeks unless stated otherwise (n=5 mice/group). For *in vivo* viral transduction (17), mice were injected via tail vein with purified adeno-associated viral vector serotype 8 (AAV8) containing a liver-specific thyroxine-binding globulin (TBG) promoter driving H19 gene expression at 5×10^{10} virus particles per mouse. Sham and BDL surgeries were performed for one week post-AAV8-null or AAV8-H19 transduction for one month, using our established method (3). For rescue experiments, mice with H19 overexpression for one month were injected via tail vein with mouse pShuttle-ZEB1 overexpression plasmid (GeneCopoeia, USA), EpCAM shRNA plasmid (Sigma-Aldrich, USA), or control plasmid at 50 μg per mouse using TurboFect *in vivo* Transfection Reagent (R0541; Thermo Scientific, Waltham, MA) as described previously (18). All mice were sacrificed after overnight fasting unless otherwise indicated. Basic procedures to analyze animal metabolic phenotypes and serum parameters were described previously (19). The hepatic bile acid (BA) pool, intestine bile pool, fecal BA excretion and serum BA concentration were measured with a Colorimetric Total Bile Acid Assay Kit (CELL BIOLABS, Inc) as described previously (20). Hematoxylin and Eosin (H&E) and Masson Trichrome staining were performed and eight fields of each slide were randomly taken under microscope and quantified by ImageJ software as described previously (5). Protocols for animal use were approved by IACUC at the University of Connecticut.

The coded normal human liver specimens, primary sclerosing cholangitis (PSC), and primary biliary cirrhosis (PBC) were obtained through the Liver Tissue Cell Distribution System (Minneapolis, Minnesota), which was funded by NIH Contract # HSN276201200017C. The patient information of PBCs and PSCs were shown in Table S1. Because we did not ascertain individual identities associated with the samples, the Institutional Review Board for Human Research at the University of Connecticut determined that the project was not research involving human subjects.

Cell lines, plasmids and antibodies

Human hepatoma cell line HepG2 (5), Huh7 (21), Hep3B (22), mouse hepatoma cell line Hepa1 (23), human embryonic kidney 293T (24), mouse large cholangiocytes (MLC), mouse small cholangiocytes (MSC) (25), human immortalized, non-malignant cholangiocyte cell line (H69), and four human cholangiocarcinoma (CCA) cell lines (Mz-Cha-1, CCLP-1, HuCC-T1 and SG231) with different biliary origin (26) were described previously. ZEB1 3′UTR luciferase construct was obtained from Addgene (6). ZEB1 CRISPR activator and CRISPR KO constructs were purchased from Santa Cruz. Epcam-Luc construct was kindly provided by Dr. Xinwei Wang (National Cancer Institute, NIH) (27). The mutant plasmid was constructed in our laboratory using Q5 Site-Directed Mutagenesis Kit (NEB, USA) (28). The antibodies were purchased from Sigma-Aldrich (ZEB1, α-SMA), Abcam (EpCAM), Cell Signaling (p-Akt, Akt, p-ERK, ERK, SMAD2/3, β-Actin), and Santa Cruz (α-Tubulin). Transcription factor and promoter interaction was predicted by Jaspar (http://jaspar.genereg.net/). RNA pull-down was performed as recently described (20).

Other standard methods

RNA isolation, qPCR, cell culture, *in vitro* virus transduction and plasmid transfection, Western blot (WB), and confocal imaging were described previously (17, 29–31). Chromatin immunoprecipitation-quantitative PCR (CHIP-qPCR), transient transfection, and luciferase reporter assay were described previously (3, 20, 32, 33). For WB, equal amounts of proteins from five mouse livers in each group (n=5/group) were pooled, and single or duplicate loading was used. The primers used were shown in Table S2. BA composition was analyzed using liquid chromatography-tandem mass spectrometry (LC-MS/MS), as described previously (20). Detailed methods can be found in Supplementary Materials.

Statistical Analysis

Data are shown as the mean ± standard error of the mean (SEM) and are representative of at least three independent experiments. Statistical analysis was carried out using Student's t test between two groups and one way ANOVA among multiple groups. $P<0.05$ was considered statistically significant.

Results

H19 overexpression facilitated the development of obstructive cholestatic liver fibrosis

To elucidate the *in vivo* function of H19 in BDL induced-cholestatic liver fibrosis, we generated H19 overexpressed mouse models via tail vein injection of AAV8-H19 or AAV8-Null (scramble control) virus driven by a specific promoter thyroxine binding globulin

(TBG) for hepatic-directed delivery (Fig. S1); an established approach with long-lasting effect without toxicity.

It was well characterized that WT mice subjected to BDL for 14 days developed severe cholestatic liver fibrosis (5). We conducted sham or BDL surgery on Null and H19 mice for 7 days in order to determine whether H19 worsened BDL-induced liver injury. H&E staining revealed liver necrosis in Null-BDL mice, which was exacerbated in H19-BDL mice (Fig. 1A, left). In addition, severe liver fibrosis and bile-duct proliferation were observed in H19-BDL vs Null-BDL mice, as determined by Trichrome Masson and Sirius Red staining (Fig. 1A, right and Fig. S2) and quantified by ImageJ (Fig. 1B). H19 mRNA was induced by BDL and the expression of fibrogenic genes Col1a1 and Col1a2 was noticeably increased by BDL vs sham in Null mice and was further elevated in H19 BDL mice (Fig. 1C).

Serum aspartate aminotransferase (AST), alanine aminotransferase (ALT), total bilirubin and direct bilirubin levels were significantly higher in Null BDL vs Null sham mice, which remained at high levels or were further increased, but to various extents, in H19 BDL vs Null BDL mice (Fig. 1D). Serum BA and BA pool size were also largely increased in Null BDL vs Null sham mice and were further elevated in H19 BDL mice (Fig. 1E). In contrast, fecal BA excretion and intestine BA levels were lower in Null BDL vs Null sham mice. Interestingly, H19 sham mice had decreased fecal BA secretion but showed much higher levels of intestine BA; both of which were decreased in H19 BDL mice. Overall, the results suggested that overexpression of H19 exacerbated BDL-induced obstructive cholestatic liver fibrosis by disrupting BA homeostasis.

H19 induced EpCAM but inhibited ZEB1 expression in BDL mice

To elucidate the molecular basis by which H19 disrupted BA homeostasis, we analyzed major regulators in the BA synthesis pathways. The mRNA expression of farnesoid X receptor (Fxr) and fibroblast growth factor receptor 4 (Fgfr4) was induced by BDL in Null mice vs sham control, however, such induction was blunted in H19 BDL compared with Null BDL mice (Fig. 2A). Cyp7a1, a rate limiting enzyme in BA synthesis, showed an expression pattern similar to Fxr and Fgfr4. Interestingly, two other BA synthetic enzymes Cyp8b1 and Cyp7b1 exhibited expression patterns distinct from that of Cyp7a1; they were induced in H19 sham vs Null sham but decreased in both Null BDL and H19 BDL mice. Although Shp is a Fxr target gene, its expression was downregulated in Null BDL vs Null Sham mice. Several genes in multiple signaling pathways also displayed noticeable changes. Specifically, EpCAM, FBJ osteosarcoma oncogene (Fos), chemokine (C-C motif) receptor 2 (Ccr2), cytokeratin 19 (Ck19), and cytokeratin 7 (Ck7) were all activated in Null BDL vs Null sham and further activated in H19 BDL relative to Null BDL (Fig. 2B).

Western blot revealed a modest elevation of α-SMA protein in Null BDL vs Null sham, but a greater induction in H19 BDL (Fig. 2C); the latter was consistent with a more severe fibrosis observed in these mice. The expression pattern of EpCAM and SRY (sex determining region Y)-box 9 (SOX9) proteins was similar to α-SMA protein, suggesting their positive association with fibrosis in H19 BDL. On the contrary, ZEB1 protein was diminished in H19 sham vs Null sham, which remained at constant low levels in H19 BDL vs Null BDL. p-ERK protein was also elevated in H19 BDL. Interestingly, the expression of

AKT and SMAD2/3 proteins did not show significant changes in H19 BDL vs Null BDL mice (Fig. S3). Considering the transcriptional function of ZEB1, we reasoned that the decreased ZEB1 may be associated with the upregulation of EpCAM in H19 BDL mice.

Another important observation was significant immuno-cell infiltration in H19-BDL mice (Fig. 2D). FACS analysis of subsets of immune components revealed that CD3+γδ+ cell population in livers and spleens from H19-BDL mice was markedly enriched compared with Null-BDL mice (Fig. 2E–2F and Fig. S4). IL-4 and IL-17 producing CD4+ and CD8+ cell populations in livers and spleens from H19-BDL mice were also up-regulated vs Null-BDL mice. There was no difference in IFN-γ producing CD4+ and CD8+ cell populations in livers of both groups, although IFN-γ producing CD8+ cell population in spleens of H19-BDL mice was upregulated. In addition, Foxp3+CD4+Treg subpopulation had no difference between H19-BDL and Null-BDL mice. The results suggest a potential important role of H19 in regulating hepatic immunoresponse.

H19 impeded ZEB1-mediated transcriptional inhibition of EpCAM

To elucidate the regulation of EpCAM by ZEB1, we overexpressed ZEB1 in human HepG2 cells and observed a reduction of EpCAM protein and mRNA by ZEB1 (Fig. 3A). Because the transfection efficiency of HepG2 cells was low, we used mouse Hepa1 and human Huh7 cells for knockdown experiments. Both EpCAM protein and mRNA were markedly induced in Hepa1 and Huh7 cells transfected with shZEB1 compared to controls (−), and a more striking effect was observed in Huh7 cells (Fig. 3B). The results suggested that ZEB1 inhibited EpCAM expression, likely at the transcriptional level.

We analyzed EpCAM promoter and identified two putative ZEB1 binding sites within the proximal promoter region (Fig. 3C, left). ChIP assays revealed a marked enrichment of ZEB1 protein to both site 1 and site 2 in the endogenous Epcam promoter in Huh7 cells (Fig. 3C, right). Interestingly, overexpression of H19 inhibited ZEB1 binding to site 1 without affecting its binding to site 2, suggesting a site-dependent selectivity. We next conducted RNA-pull down assays combined with WB. *In vitro* transcribed *H19*RNA probe and negative control (NC) RNA probe were incubated with Hepa1 cell lysis to detect the interaction between *H19*RNA and the endogenous ZEB1 protein. The result showed that the *H19*RNA probe recruited a significant amount of ZEB1 protein than NC, indicating an association between H19 and ZEB1 (Fig. 3D). Thus, the direct *H19*RNA-ZEB1 protein interaction likely resulted in dissociation of ZEB1 protein from site1 in the EpCAM promoter.

Promoter luciferase reporter assays further demonstrated that overexpression of H19 activated whereas overexpression of ZEB1 reduced EpCAM promoter activities by H19 in Hepa1 and Huh7 cells (Fig. 3E, left two panels). In contrast, the effect of H19 was completely blunted and the inhibition of ZEB1 was largely impaired when site 1 was mutated in the EpCAM promoter (Fig. 3E, right two panels). We subsequently examined EpCAM promoter activity in two additional cell lines 293T and Hep3B cells and observed an inhibition by ZEB1 overexpression and activation by knockdown of ZEB1 (Fig. 3F). Taken together, these results provided convincing evidence that ZEB1 served as a

transcriptional repressor of EpCAM expression and that H19 activated EpCAM by dissociating ZEB1 from the EpCAM promoter.

Overexpression of ZEB1 or knockdown of EpCAM alleviated fibrosis in H19 BDL mice

We conducted rescue experiments to dissect out the role of ZEB1 and EpCAM in H19-mediated cholestatic fibrosis. Mice transduced with AAV8-H19 for 1 month were injected with Zeb1, shEpcam, or control plasmid via tail vein for 1 day followed by BDL for 7 days. H&E and Masson Trichrome staining revealed significantly attenuated fibrosis in H19-Zeb1-BDL and H19-shEpcam-BDL mice compared to H19-Con-BDL mice (Fig. 4A). The reduced liver injury was accompanied by the decreased serum ALT, AST, and bilirubin levels (Fig. 4B).

Interestingly, hepatic *H19*RNA was decreased in shEpcam-BDL mice, suggesting a potential feedback activation of H19 by EpCAM (Fig. 4B). As expected, Epcam mRNA was reduced in Zeb1-BDL mice. In addition, the expression of cholangiocyte markers (Ck7, Ck19) and fibrosis markers (Col1a1, Col1a2, α-Sma) was markedly decreased in Zeb1-BDL and shEpcam-BDL mice.

Western blot confirmed the decreased EpCAM proteins in Zeb1-BDL livers (Fig. 4C), providing *in vivo* evidence that EpCAM was the direct target of ZEB1. It was noted that ZEB1 proteins remained unchanged in shEpcam-BDL mice (Fig. 4D), suggesting that Epcam was the downstream gene responsible for promoting cholestatic liver fibrosis. As expected, SOX9 and α-SMA proteins were decreased in both Zeb1-BDL and shEpcam-BDL mice. The survival curve showed that the mortality rates of H19-Zeb1-BDL and H19-shEpcam-BDL mice were markedly lower than that of H19-BDL mice (Fig. 4E). Analysis of serum bile acid composition revealed decreased levels of cholic acid (CA), taurodeoxycholic acid (TDCA), glycochenodeoxycholic acid (GCDCA), tauroursodeoxycholic acid (TUDCA), and glycoursodeoxycholic acid (GUDCA) in Zeb1 and shEpcam mice compared to H19 mice (Fig. 4F). In addition, CDCA-derived alpha-muricholic acid (αMCA) and its conjugate TαMCA were also decreased in Zeb1 and shEpcam mice. Beta-muricholic acid (βMCA) and its derived omega-muricholic acid (ωMCA) were only diminished in Zeb1 but not in shEpcam mice. Overall, either overexpression of ZEB1 or knockdown of EpCAM rescued liver fibrosis induced by H19 by altering BA composition.

H19-deficiency prevented cholestatic liver fibrosis

We further elucidated the role of H19 in BDL-induced cholestasis by using $H19^{-/-}$ mice. As a paternal imprinted gene, mice with *H19*-deficiency from the maternal chromosome were $H19^{-/-}$ mice whereas mice with *H19*-deficiency from the paternal chromosome were used as negative controls. Because 10 week-old WT (Null) mice underwent BDL for 7 days showed less severe liver fibrosis (Fig. S1 and Fig. 1A), we used 22 week-old mice for this experiment in order to observe more significant differences between the control and $H19^{-/-}$ mice. As expected, H&E and Masson Trichrome staining revealed a marked reduction in liver injury and periductular fibrosis in $H19^{-/-}$ vs control mice (Fig. 5A), which was accompanied by the decreased levels of serum AST, ALT, bilirubin, and BA (Fig. 5B). Consistently, the protein (Fig. 5C) and mRNA (Fig. 5D) levels of ZEB1 were increased

whereas EPCAM and SOX9 were decreased in *H19*$^{-/-}$ mice. In addition, the expression of Ck7, Ck19, Col1a1, Col1a2, and α-Sma was concomitantly reduced in *H19*$^{-/-}$ livers (Fig. 5D). However, EMT related genes showed minimal changes in H19$^{-/-}$ vs control livers (Fig. S5).

Overall, the results provided direct *in vivo* evidence for a regulatory role of H19 in cholestatic liver fibrosis.

Bile acids induced H19 in cholangiocytes to control ZEB1 and EpCAM expression

One major phenotype in H19-BDL mice was the development of periductular fibrosis (Fig. 4A), thus we determined the H19/ZEB1/EpCAM regulation in cholangiocytes. We examined H19 expression regulation by various BAs in small (MSC) and large (MLC) mouse cholangiocytes. It was interesting to note that *H19*RNA was highly induced by several BAs, including CA, TCA, UDCA and LCA (5~15 fold induction) in MSC but was only modestly induced by TCA and UDCA (~1.5 fold induction) in MLC (Fig. 6A). However, *H19*RNA was only induced by LCA in primary hepatocytes of WT but not *H19*$^{-/-}$ mice (Fig. S6). Overexpression of H19 markedly reduced ZEB1 protein with a concurrent induction of EpCAM in MSC (Fig. 6B). Interestingly, H19 showed no effect in ZEB1 expression in MLC in which EpCAM protein could not be detected with a short exposure time.

To establish the clinical relevance of H19 in cholestasis, we examined the effect of H19 in several human cholangiocyte cell lines, including human normal cholangiocyte cell line (H69) and cholangiocarcinoma cell lines (SG231, HuCC-T1, CCLP-1, Mz-Cha-1). Overexpression of H19 markedly induced EPCAM with a moderate reduction of ZEB1 in H69 (Fig. 6C). In SG231, H19 moderately elevated EPCAM without affecting ZEB1 protein. In HuCCT-1, H19 moderately decreased ZEB1 with a commitment induction of EPCAM. In CCLP-1, H19 markedly diminished ZEB1 and induced EPCAM. In Mz-Cha-1 cells, H19 inhibited EPCAM although ZEB1 was not detected. The molecular basis for the differential responses of mouse and human cholangiocytes to H19 was unclear as the endogenous *H19*RNA was much higher in MLS and CCLP-1 (Fig. S7A–S7B). Nonetheless, the results suggested that H19 activation of EPCAM expression could be either dependent or independent of ZEB1 reduction in different cholangiocarcinoma cell lines.

Hepatic H19 and EpCAM were upregulated in human cholestatic liver fibrosis

PSC and PBC are the most common immune-mediated chronic cholestatic liver fibrosis. In PSC, bile ducts become blocked, leading to bile accumulation in the liver that slowly damages the bile ducts. The focal lesion typical for PSC is periductular layered fibrosis (characteristic “onion skin” pattern) seen with edema and inflammation surrounding the interlobular bile ducts (34). As shown above, a similar characteristic was observed in H19-BDL mice (Fig. 4A). PBC is a chronic autoimmune liver disease characterized by progressive destruction of the bile ducts and cholestasis. We determined *H19*RNA levels in normal, PSC, and PBC liver specimens and observed markedly elevated H19 expression in PSC and PBC (Fig. 6D). We divided the samples into two groups based on the relative levels of H19 vs the normal samples, namely “H19 high” and “H19 low”. EpCAM proteins were significantly induced in PSC in both groups but were more highly induced in PBC in “H19

high" vs "H19 low" (Fig. 6E). The decreased ZEB1 proteins were observed in PSC and PBC of the "H19 high" group compared to normal, which was negatively correlated with EpCAM expression. Interestingly, CK19 proteins were only elevated in PSC but not PBC in the "H19 high group". Taken together, the results strongly support the involvement of H19 in the pathogenesis of human cholestatic liver fibrosis.

Discussion

Albeit from different origins including biliary obstruction, infection of hepatitis virus, alcohol consumption, and non-alcoholic steatohepatitis, liver fibrosis can progress into cirrhosis and ultimately into end-stage liver diseases. Accumulating progresses have been made to better understand the underlying mechanisms of hepatic fibrosis with recent major investigation focused on the dynamic homeostasis between hepatic progenitor cells and ductular reaction, balance of epithelial cell niche and mesenchymal cell niche (35). As one of the earliest discovered lncRNAs, H19 has been recognized as a multi-functional regulator, including orchestrating the epithelial-to-mesenchymal transition (EMT) to promote tumor growth (36). In this study, we unravel a crucial function of H19 in cholestatic liver diseases. We demonstrate that hepatic overexpression of H19 exacerbates whereas *H19*-deficiency ameliorates obstructive cholestatic liver fibrosis.

We identify EpCAM as a novel downstream target gene of ZEB1. ZEB1 represses EpCAM gene transcription by the direct binding to the EpCAM promoter and H19 suppresses ZEB1 transactivation by interacting with ZEB1 to prevent its binding. Mechanistically, H19 promotes fibrosis at least in part through its activation of EpCAM by downregulating ZEB1 in both hepatocytes and cholangiocytes. Thus, we elucidate a dual inhibitory mechanism involving H19 repression of ZEB1 and ZEB1 inhibition of EpCAM, leading to EpCAM activation by H19 (Fig. 7).

This dual inhibitory mechanism is further supported by *in vivo* studies. Either overexpression of ZEB1 or knockdown of EpCAM hampers H19-induced periductular fibrosis. However, EpCAM is diminished in ZEB1 mice whereas ZEB1 remains unaltered in shEpCAM mice, demonstrating EpCAM is downstream of ZEB1 to dictate H19-mediated fibrosis. Because EpCAM is also used as a marker of biliary hyperplasia (37), the activation of EpCAM by H19 likely contributes to the ductular reaction. A recent study reported that ZEB1 is neither required nor sufficient for EMT in LS174T colorectal cancer cells lacking endogenous EMT-inducing transcription factors (38). In our studies, H19 markedly diminishes ZEB1 in MSC cells that express high levels of EpCAM but has no effect on downregulating ZEB1 in MLC cells which contain low levels of EpCAM. On the other hand, *H19*RNA is diminished in ShEpCAM mice, which could be due to alleviated liver injury and decreased BA levels.

Electron microscopic studies in rodent liver sections and intrahepatic bile duct units (IBDUs) have demonstrated that small cholangiocytes show a high nucleus-to-cytoplasm ratio and represent a hepatic progenitor cell population (34). It was reported that hepatic progenitors cells (HPCs) are the source of proliferating biliary epithelial cells in BDL-induced liver fibrosis (39). Consistently, H19 appeared to be more effective in small

cholangicytes other than large cholangiocytes. Therefore HPCs may also be involved in the pathological process of H19-induced liver fibrosis.

It is noted that in human CCA cell line Mz-Cha-1, the activation of EpCAM by H19 occurs in the absence of ZEB1. H19 also induces EpCAM without affecting ZEB1 levels in SG231 cells. Therefore, H19 likely induces EpCAM via alternative mechanisms independent of ZEB1 in both cells. Impressively, the elevated EpCAM correlates with downregulated ZEB1 expression in human PSC and PBC expressing high levels of H19, providing clinical evidence for an important role of H19 in mediating the development of bililary fibrosis.

α-SMA is one of the most reliable markers of stellate cell (HSC) activation. It is increasingly used as an early indication of fibrogenic activity in human liver disease, even before extracellular matrix accumulates (22). The expression of α-SMA protein was elevated in H19-BDL mice and decreased in *H19*$^{-/-}$-BDL mice, suggesting that the activation of HSCs also contributed to H19-mediated fibrosis.

In summary, our study reveals a novel function of H19 as a profibrotic mediator of cholestatic live fibrosis. The dysregulation of bile acid homeostasis results in a marked induction of H19 by bile acids in cholangiocytes and hepatocytes, and this in turn prevents ZEB1 inhibition of EpCAM, causing EpCAM activation and leading to biliary hyperplasia. Our work provides new mechanistic insight into the role of lncRNA in cholestatic live fibrosis and may pave the way for the development of therapeutic strategies to target lncRNA.

Supplementary Material

Refer to Web version on PubMed Central for supplementary material.

Acknowledgments

Grant Support: L. Wang is supported by NIH R01DK104656, R01DK080440, R01ES025909, R21AA022482, R21AA024935, VA Merit Award 1I01BX002634, P30 DK34989 (Yale Liver Center) and the National Natural Scientific Foundation of China (Grant No. 81572443). OB is supported by grants from the Canadian Institute of Health Research (CIHR; grant#119331), the Canadian Foundation for Innovation (CFI; grant#25712), the Canadian Liver Foundation and the Natural Sciences and Engineering Research Council of Canada (NSERC).

We appreciate Dr. Xinwei Wang (National Cancer Institute, NIH) for the Epcam-Luc construct and Dr. Meenakshisundaram Ananthanarayanan (Yale University) for cholangiocyte-derived cells.

List of Abbreviations

AAV8	adeno-associated viral vector serotype 8
ALT	alanine aminotransferase
AST	Aspartate aminotransferase
α-SMA	alpha smooth muscle actin
BA	bile acids
BDL	bile-duct ligation

CCR2	C-C motif chemokine receptor 2
CK7	cytokeratin7
CK19	cytokeratin19
Col1a1	collagen type I alpha 1
Col1a2	collagen type I alpha 2
EpCAM	epithelial cell adhesion molecule
FGFR4	fibroblast growth factor receptor 4
FXR	farnesoid X receptor
IHC	immunohistochemistry
lncRNA	long non-coding RNA
PBC	primary biliary cirrhosis
PSC	primary sclerosing cholangitis
SOX9	SRY (sex determining region Y)-box 9
ZEB1	Zinc finger E-box-binding homeobox 1

References

1. Wang L, Lee YK, Bundman D, Han Y, Thevananther S, Kim CS, Chua SS, et al. Redundant pathways for negative feedback regulation of bile acid production. Dev Cell. 2002; 2:721–731. [PubMed: 12062085]
2. Chiang JY. Bile acids: regulation of synthesis. J Lipid Res. 2009; 50:1955–1966. [PubMed: 19346330]
3. Zhang Y, Xu N, Xu J, Kong B, Copple B, Guo GL, Wang L. E2F1 is a novel fibrogenic gene that regulates cholestatic liver fibrosis through the Egr-1/SHP/EID1 network. Hepatology. 2014; 60:919–930. [PubMed: 24619556]
4. Ratajczak MZ. Igf2-H19, an imprinted tandem gene, is an important regulator of embryonic development, a guardian of proliferation of adult pluripotent stem cells, a regulator of longevity, and a 'passkey' to cancerogenesis. Folia Histochem Cytobiol. 2012; 50:171–179. [PubMed: 22763974]
5. Zhang Y, Liu C, Barbier O, Smalling R, Tsuchiya H, Lee S, Delker D, et al. Bcl2 is a critical regulator of bile acid homeostasis by dictating Shp and lncRNA H19 function. Sci Rep. 2016; 6:20559. [PubMed: 26838806]
6. Gregory PA, Bert AG, Paterson EL, Barry SC, Tsykin A, Farshid G, Vadas MA, et al. The miR-200 family and miR-205 regulate epithelial to mesenchymal transition by targeting ZEB1 and SIP1. Nat Cell Biol. 2008; 10:593–601. [PubMed: 18376396]
7. Larsen JE, Nathan V, Osborne JK, Farrow RK, Deb D, Sullivan JP, Dospoy PD, et al. ZEB1 drives epithelial-to-mesenchymal transition in lung cancer. J Clin Invest. 2016; 126:3219–3235. [PubMed: 27500490]
8. Zhang Y, Yang Z, Whitby R, Wang L. Regulation of miR-200c by nuclear receptors PPARalpha, LRH-1 and SHP. Biochem Biophys Res Commun. 2011; 416:135–139. [PubMed: 22100809]
9. Zhang Y, Hagedorn CH, Wang L. Role of nuclear receptor SHP in metabolism and cancer. Biochim Biophys Acta. 2011; 1812:893–908. [PubMed: 20970497]

10. Rudraiah S, Zhang X, Wang L. Nuclear Receptors as Therapeutic Targets in Liver Disease: Are We There Yet? Annu Rev Pharmacol Toxicol. 2016; 56:605–626. [PubMed: 26738480]
11. Matouk IJ, Halle D, Raveh E, Gilon M, Sorin V, Hochberg A. The role of the oncofetal H19 lncRNA in tumor metastasis: orchestrating the EMT-MET decision. Oncotarget. 2015
12. Dolle L, Theise ND, Schmelzer E, Boulter L, Gires O, van Grunsven LA. EpCAM and the biology of hepatic stem/progenitor cells. Am J Physiol Gastrointest Liver Physiol. 2015; 308:G233–250. [PubMed: 25477371]
13. Mani SK, Zhang H, Diab A, Pascuzzi PE, Lefrancois L, Fares N, Bancel B, et al. EpCAM-Regulated Intramembrane Proteolysis Induces a Cancer Stem Cell-like Gene Signature in Hepatitis B Virus-infected Hepatocytes. J Hepatol. 2016
14. Maetzel D, Denzel S, Mack B, Canis M, Went P, Benk M, Kieu C, et al. Nuclear signalling by tumour-associated antigen EpCAM. Nat Cell Biol. 2009; 11:162–171. [PubMed: 19136966]
15. Uehara T, Ainslie GR, Kutanzi K, Pogribny IP, Muskhelishvili L, Izawa T, Yamate J, et al. Molecular mechanisms of fibrosis-associated promotion of liver carcinogenesis. Toxicol Sci. 2013; 132:53–63. [PubMed: 23288052]
16. Venkatraman A, He XC, Thorvaldsen JL, Sugimura R, Perry JM, Tao F, Zhao M, et al. Maternal imprinting at the H19-Igf2 locus maintains adult haematopoietic stem cell quiescence. Nature. 2013; 500:345–349. [PubMed: 23863936]
17. Lee SM, Zhang Y, Tsuchiya H, Smalling R, Jetten AM, Wang L. Small heterodimer partner/neuronal PAS domain protein 2 axis regulates the oscillation of liver lipid metabolism. Hepatology. 2015; 61:497–505. [PubMed: 25212631]
18. Yang Z, Tsuchiya H, Zhang Y, Lee S, Liu C, Huang Y, Vargas GM, et al. REV-ERBalpha Activates C/EBP Homologous Protein to Control Small Heterodimer Partner-Mediated Oscillation of Alcoholic Fatty Liver. Am J Pathol. 2016; 186:2909–2920. [PubMed: 27664470]
19. Tabbi-Anneni I, Cooksey R, Gunda V, Liu S, Mueller A, Song G, McClain DA, et al. Overexpression of nuclear receptor SHP in adipose tissues affects diet-induced obesity and adaptive thermogenesis. Am J Physiol Endocrinol Metab. 2010; 298:E961–970. [PubMed: 20124506]
20. Zhang L, Yang Z, Trottier J, Barbier O, Wang L. Long noncoding RNA MEG3 induces cholestatic liver injury by interaction with PTBP1 to facilitate shp mRNA decay. Hepatology. 2017; 65:604–615. [PubMed: 27770549]
21. Zhang Y, Wang L. Nuclear receptor SHP inhibition of Dnmt1 expression via ERRgamma. FEBS Lett. 2011; 585:1269–1275. [PubMed: 21459093]
22. Yang Z, Koehler AN, Wang L. A Novel Small Molecule Activator of Nuclear Receptor SHP Inhibits HCC Cell Migration via Suppressing Ccl2. Mol Cancer Ther. 2016; 15:2294–2301. [PubMed: 27486225]
23. Zhou T, Zhang Y, Macchiarulo A, Yang Z, Cellanetti M, Coto E, Xu P, et al. Novel polymorphisms of nuclear receptor SHP associated with functional and structural changes. J Biol Chem. 2010; 285:24871–24881. [PubMed: 20516075]
24. Yang Z, Wang L. An autoregulatory feedback loop between Mdm2 and SHP that fine tunes Mdm2 and SHP stability. FEBS Lett. 2012; 586:1135–1140. [PubMed: 22575647]
25. Woo K, Sathe M, Kresge C, Esser V, Ueno Y, Venter J, Glaser SS, et al. Adenosine triphosphate release and purinergic (P2) receptor-mediated secretion in small and large mouse cholangiocytes. Hepatology. 2010; 52:1819–1828. [PubMed: 20827720]
26. Han Y, Meng F, Venter J, Wu N, Wan Y, Standeford H, Francis H, et al. miR-34a-dependent overexpression of Per1 decreases cholangiocarcinoma growth. J Hepatol. 2016; 64:1295–1304. [PubMed: 26923637]
27. Huang Y, Ma C, Zhang Q, Ye J, Wang F, Zhang Y, Hunborg P, et al. CD4+ and CD8+ T cells have opposing roles in breast cancer progression and outcome. Oncotarget. 2015; 6:17462–17478. [PubMed: 25968569]
28. Yang Z, Zhang Y, Wang L. A feedback inhibition between miRNA-127 and TGFbeta/c-Jun cascade in HCC cell migration via MMP13. PLoS One. 2013; 8:e65256. [PubMed: 23762330]

29. Tsuchiya H, da Costa KA, Lee S, Renga B, Jaeschke H, Yang Z, Orena SJ, et al. Interactions Between Nuclear Receptor SHP and FOXA1 Maintain Oscillatory Homocysteine Homeostasis in Mice. Gastroenterology. 2015; 148:1012–1023. e1014. [PubMed: 25701738]
30. Lua I, James D, Wang J, Wang KS, Asahina K. Mesodermal mesenchymal cells give rise to myofibroblasts, but not epithelial cells, in mouse liver injury. Hepatology. 2014; 60:311–322. [PubMed: 24488807]
31. Yoon SM, Gerasimidou D, Kuwahara R, Hytiroglou P, Yoo JE, Park YN, Theise ND. Epithelial cell adhesion molecule (EpCAM) marks hepatocytes newly derived from stem/progenitor cells in humans. Hepatology. 2011; 53:964–973. [PubMed: 21319194]
32. Zhang Y, Andrews GK, Wang L. Zinc-induced Dnmt1 expression involves antagonism between MTF-1 and nuclear receptor SHP. Nucleic Acids Res. 2012; 40:4850–4860. [PubMed: 22362755]
33. Yang Z, Tsuchiya H, Zhang Y, Hartnett ME, Wang L. MicroRNA-433 inhibits liver cancer cell migration by repressing the protein expression and function of cAMP response element-binding protein. J Biol Chem. 2013; 288:28893–28899. [PubMed: 23979134]
34. Marchioni Beery RM, Vaziri H, Forouhar F. Primary Biliary Cirrhosis and Primary Sclerosing Cholangitis: a Review Featuring a Women's Health Perspective. J Clin Transl Hepatol. 2014; 2:266–284. [PubMed: 26357630]
35. Williams MJ, Clouston AD, Forbes SJ. Links between hepatic fibrosis, ductular reaction, and progenitor cell expansion. Gastroenterology. 2014; 146:349–356. [PubMed: 24315991]
36. Matouk IJ, DeGroot N, Mezan S, Ayesh S, Abu-lail R, Hochberg A, Galun E. The H19 non-coding RNA is essential for human tumor growth. PLoS One. 2007; 2:e845. [PubMed: 17786216]
37. Zen Y, Vara R, Portmann B, Hadzic N. Childhood hepatocellular carcinoma: a clinicopathological study of 12 cases with special reference to EpCAM. Histopathology. 2014; 64:671–682. [PubMed: 24138022]
38. Jagle S, Dertmann A, Schrempp M, Hecht A. ZEB1 is neither sufficient nor required for epithelial-mesenchymal transition in LS174T colorectal cancer cells. Biochem Biophys Res Commun. 2016
39. Michelotti GA, Tucker A, Swiderska-Syn M, Machado MV, Choi SS, Kruger L, Soderblom E, et al. Pleiotrophin regulates the ductular reaction by controlling the migration of cells in liver progenitor niches. Gut. 2016; 65:683–692. [PubMed: 25596181]

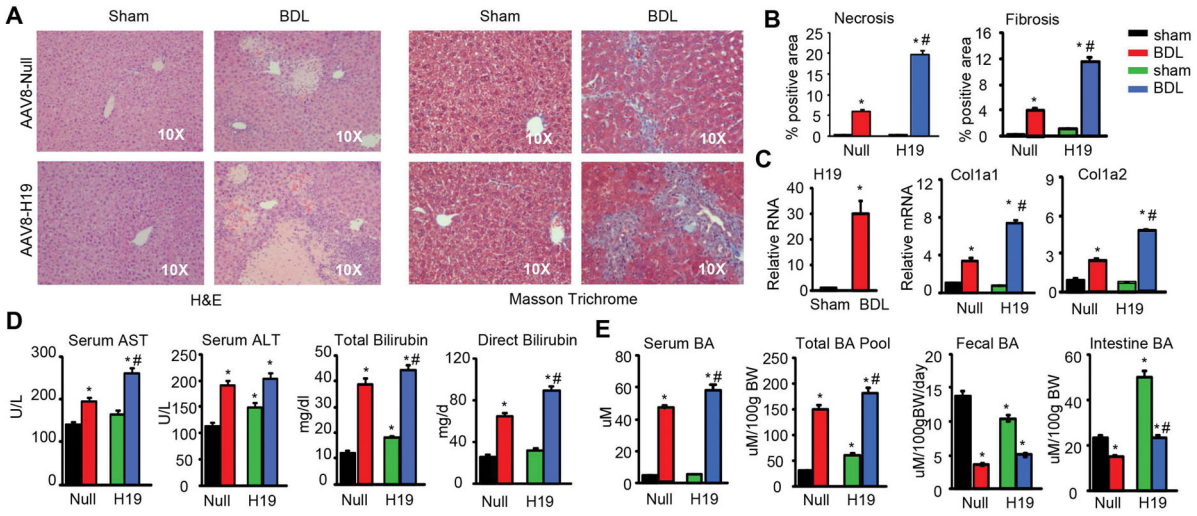

Figure 1. Hepatic expression of H19 exacerbated obstructive cholestatic liver fibrosis

(A) Representative images of H&E and Masson Trichrome staining of liver sections. C57/BL6 mice were transduced with AAV8-Null or AAV8-H19 virus via tail vein injection for 1 month followed by sham or BDL for 7 days (n=5 mice/group).

(B) Quantification of results of liver necrosis and fibrosis in A. **P*<0.01 vs Null-sham; #*P*<0.01 vs Null-BDL.

(C) qPCR of *H19*RNA and alpha I and II collagen (Col1a1, Col1a2) mRNAs in mouse livers from mice in A.

(D) Measurement of serum AST, ALT, and bilirubin levels from mice in A.

(E) Measurement of serum bile acid (BA), BA pool size, fecal BA excretion, and intestinal BA levels from mice in A.

C-E: Data are shown as mean ± SEM (n=5/group of triplicate assays). **P*<0.01 vs Null-sham; #*P*<0.01 vs Null-BDL.

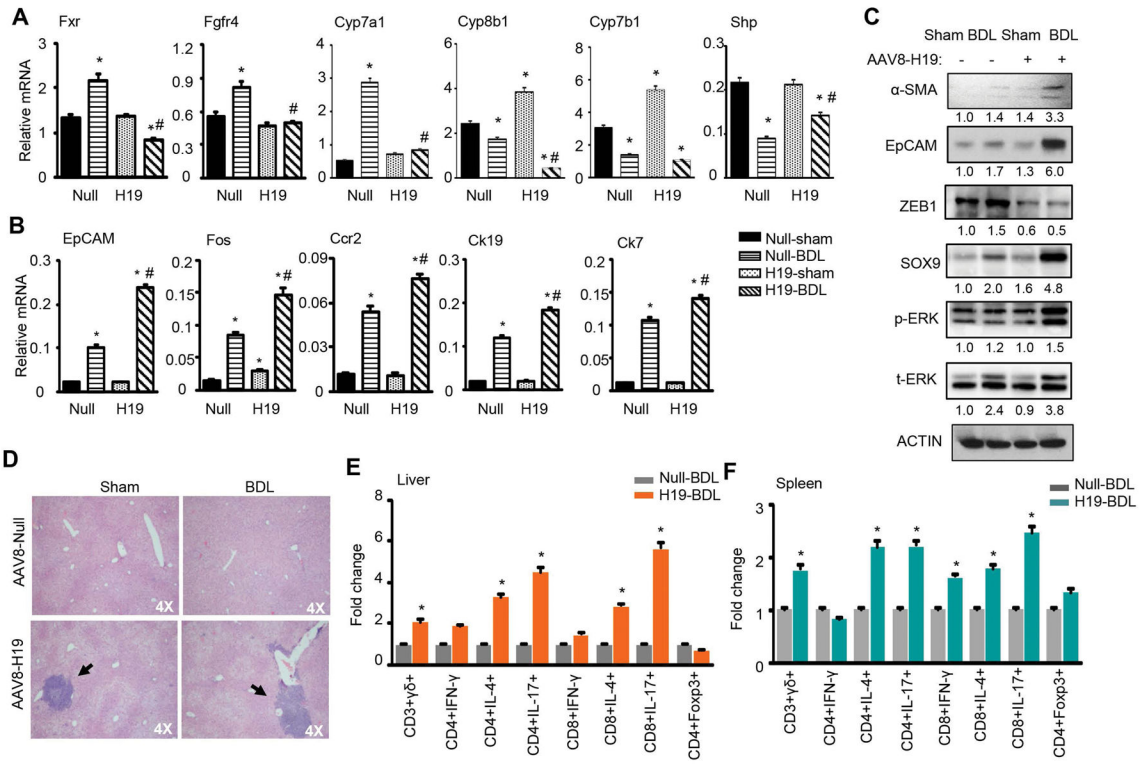

Figure 2. EpCAM was upregulated whereas ZEB1 was downregulated in H19-BDL mice

(A–B) qPCR of mRNA expression in livers of Null and H19 mice under sham or BDL for 7 days. Data are shown as mean ± SEM (n=5/group of triplicate assays). **P*<0.01 vs Null-sham; #*P*<0.01 vs Null-BDL.

(C) Western blot of protein expression in livers of Null and H19 mice under sham or BDL for 7 days. Each band represented pooled sample (equal amounts of protein) from 5 individual mice. Quantification of the intensity of each band was performed by Image J software and provided under each line.

(D) Representative images of H&E staining of liver sections.

(E–F) FACS analysis of different subsets of immune cell populations in livers (E) and spleens (F) of Null-BDL and H19-BDL mice. The results were presented as fold change of H19-BDL vs Null-BDL (**P*<0.01).

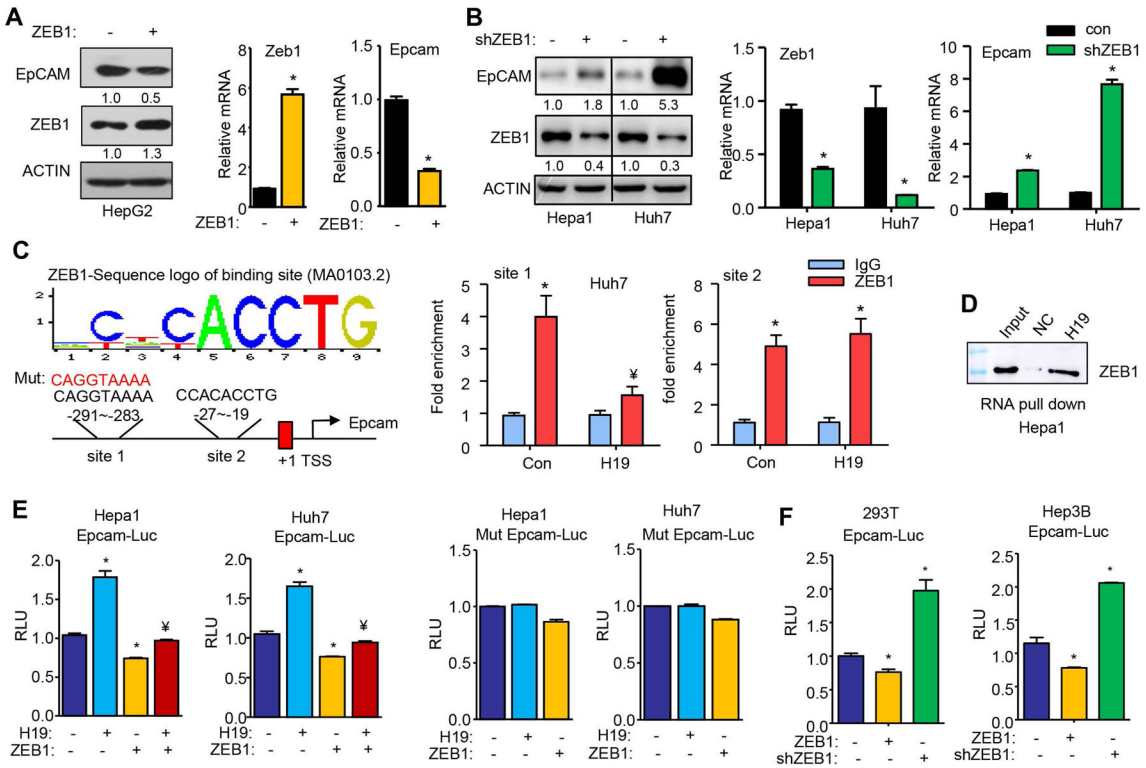

Figure 3. H19 prevented ZEB1 from binding to and inhibiting EpCAM promoter activity

(A) Western blot of protein expression and qPCR of mRNA expression in HepG2 cells with ZEB1 overexpression. The cells were transfected with ZEB1 expression plasmid for 48 hrs and total protein and mRNA were isolated. Data are shown as mean ± SEM (triplicate assays). **P*<0.01 vs con.

(B) Western blot of protein expression and qPCR of mRNA expression in Hepa1 and Huh7 cells with ZEB1 knockdown. Hepa1 and Huh7 cells were transfected with shZEB1 plasmid 48 hrs and total protein and mRNA were isolated. Data are shown as mean ± SEM (triplicate assays). **P*<0.01 vs con.

(C) Left: Diagram showing two ZEB1 binding sites identified in the Epcam promoter. Right: ChIP assays to determine the enrichment of ZEB1 protein in the endogenous EpCAM promoter and the effect of H19. Huh7 cells were transfected with AAV8-Con or AAV8-H19 virus for 48 hrs and the samples were harvested. Relative enrichment was calculated by comparing samples immunoprecipitated with IgG and ZEB1 antibodies, respectively. **P*<0.01 vs IgG, ¥*P*<0.01 vs con-ZEB1.

(D) RNA pull-down followed by Western blot to determine the direct association of *H19*RNA with ZEB1 protein in Hepa1 cells. Cell lysates of Hepa1 were incubated with biotin-labeled *H19*RNA, or a negative control (NC) transcript. After pull-down, the recruitment of ZEB1 to H19 was examined by Western blot with anti-ZEB1 antibody.

(E) Left: Transient transfection assays to determine EpCAM promoter luciferase reporter activity regulated by H19 and ZEB1. Right: Mutagenesis assays. EpCAM promoter mutant construct was generated and used for transient transfection assays. Data are shown as mean ± SEM (triplicate assays). **P*<0.01 vs con, ¥ *P*<0.01 vs H19.

(F) Transient transfection assays to determine EpCAM promoter luciferase reporter activity in the presence of ZEB1 overexpression or knockdown (shZEB1). Data are shown as mean ± SEM (triplicate assays). *P<0.01 vs con.

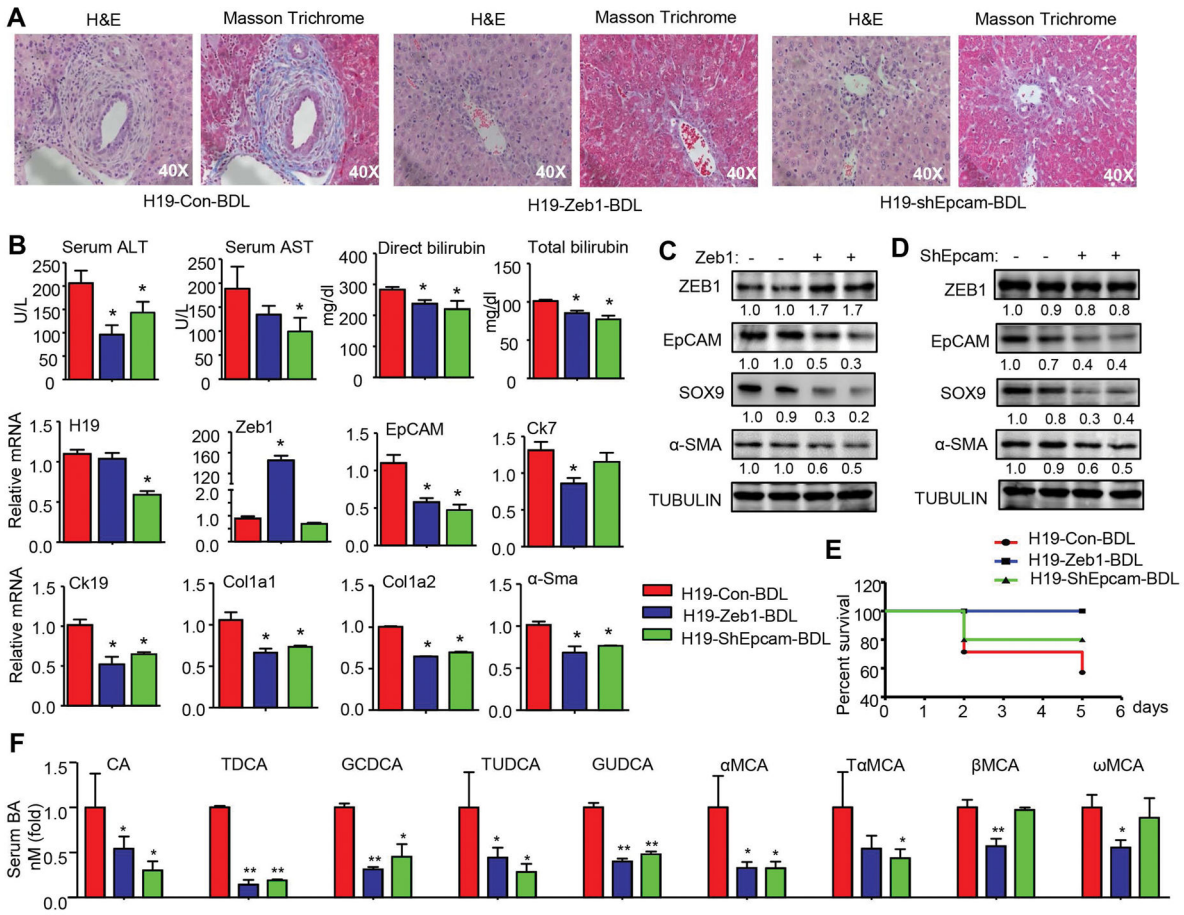

Figure 4. ZEB1 expression or EpCAM knockdown impeded liver fibrosis in H19-BDL mice

(A) Representative images of H&E and Masson Trichrome staining of liver sections. C57/BL6 mice were transduced with AAV8-H19 virus via tail vein injection for 1 month. The mice were then injected with the control plasmid, ZEB1 overexpression plasmid, or shEpCAM plasmid via the tail vein using TurboFect *in vivo* Transfection Reagent for 1 day, followed by BDL for 7 days (n=10 mice/group).

(B) Measurement of serum AST, ALT, and bilirubin levels and qPCR of mRNA expression in livers from mice in A. Data were shown as mean ± SEM (n=10/group of triplicate assays). **P*< 0.05 vs H19-Con-BDL.

(C) Western blot of protein expression in H19-Con-BDL (−) and H19-ZEB1-BDL (+) mouse livers.

(D) Western blot of protein expression in H19-Con-BDL (−) and H19-shEpCAM-BDL (+) mouse livers. C–D: Each band represented pooled sample (equal amounts of protein) from 10 individual mice and loaded in duplicate lanes. Quantification of the intensity of each band was performed by Image J software and provided under each line.

(E) Survival curve of mice in A (n=10/group). Survival curve of H19-overexpressed mice injected with ZEB1 or ShEpcam plasmids, followed by BDL 1 day later. **P*< 0.05 vs H19-Con-BDL.

(F) Serum bile acid composition analysis by LC-MS/MS from mice in A.

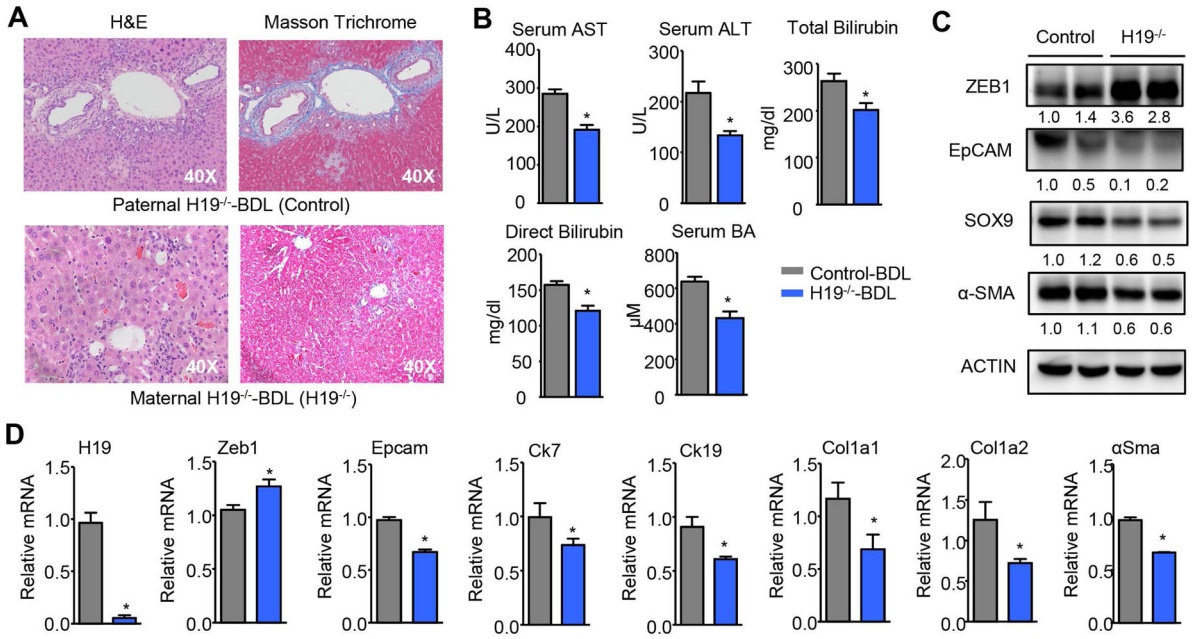

Figure 5. *H19*-deficiency alleviated obstructive cholestatic liver fibrosis

(A) Representative images of H&E and Masson Trichrome staining of liver sections from control (paternal H19$^{-/-}$) and *H19*$^{-/-}$ (maternal H19$^{-/-}$) mice underwent BDL for 7 days (n=5/group).

(B) Measurement of serum AST, ALT, bilirubin, and BA levels from mice in A. Data were shown as mean ± SEM (n=5/group of triplicate assays). **P*< 0.05 vs *H19*$^{-/-}$.

(C) Western blot of protein expression in livers from mice in A. Each band represented pooled sample (equal amounts of protein) from 5 individual mice and loaded in duplicate lanes. Quantification of the intensity of each band was performed by Image J software and provided under each line.

(D) qPCR of mRNA expression in livers from mice in A. Data were shown as mean ± SEM (n=5/group of triplicate assays). **P*< 0.05 vs *H19*$^{-/-}$.

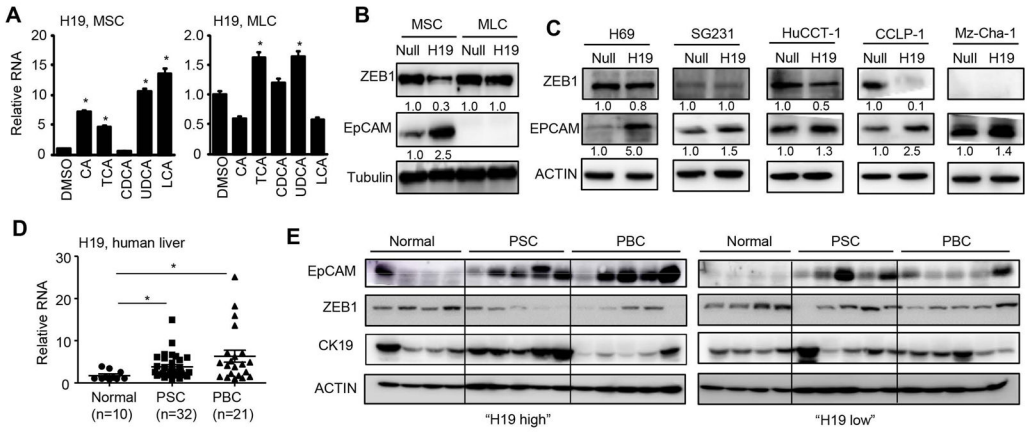

Figure 6. Bile acids induced H19 in cholangiocytes to dictate ZEB1 and EpCAM function

(A) qPCR of *H19*RNA in mouse small (MSC) and large (MLC) cholangiocytes. MSC and MLC were treated with cholic acid (CA, 100 μM), taurocholic acid (TCA, 100 μM), chenodeoxycholic acid (CDCA, 100 μM), ursodeoxycholic acid (UDCA, 100 μM) or lithocholic acid (LCA, 10 μM) for 24 hrs. Data were shown as mean ± SEM (triplicate assays). **P*< 0.05 vs DMSO.

(B) Western blot of protein expression in mouse MSC and MLC overexpressed with Null or H19 for 48 hrs.

(C) Western blot of protein expression in human H69, SG231, HuCCT-1, CCLP-1 and Mz-Cha-1 cells overexpressed with Null or H19 for 48 hrs.

(D) qPCR of *H19*RNA in normal, primary sclerosing cholangitis (PSC), and primary biliary cirrhosis (PBC) liver tissues. Data were shown as mean ± SEM (triplicate assays). **P*< 0.05 vs normal.

(E) Western blot of protein expression in human normal, PSC and PBC livers. Each lane represented an individual specimen.

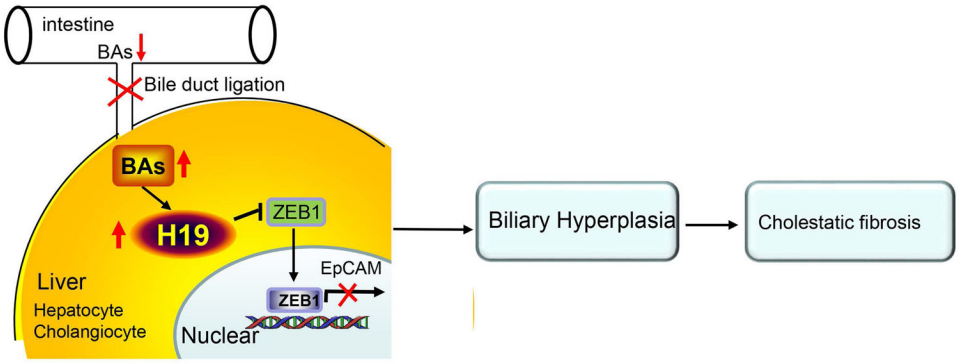

Figure 7.

Diagram showing H19-mediated expression of ZEB1 and EpCAM to control cholestatic liver fibrosis. Bile acid accumulation induced by bile duct ligation increased hepatic *H19*RNA expression. The upregulation of *H19*RNA inhibited ZEB1 expression and its binding to the EpCAM promoter, thus preventing ZEB1 from repressing EpCAM gene transcription. This in turn resulted in the upregulation of EpCAM by H19, which drove cholangiocyte proliferation and the development of cholestatic liver fibrosis.